Recent Developments in Nanofabrication Using Ion Projection Lithography

*Ampere A. Tseng**

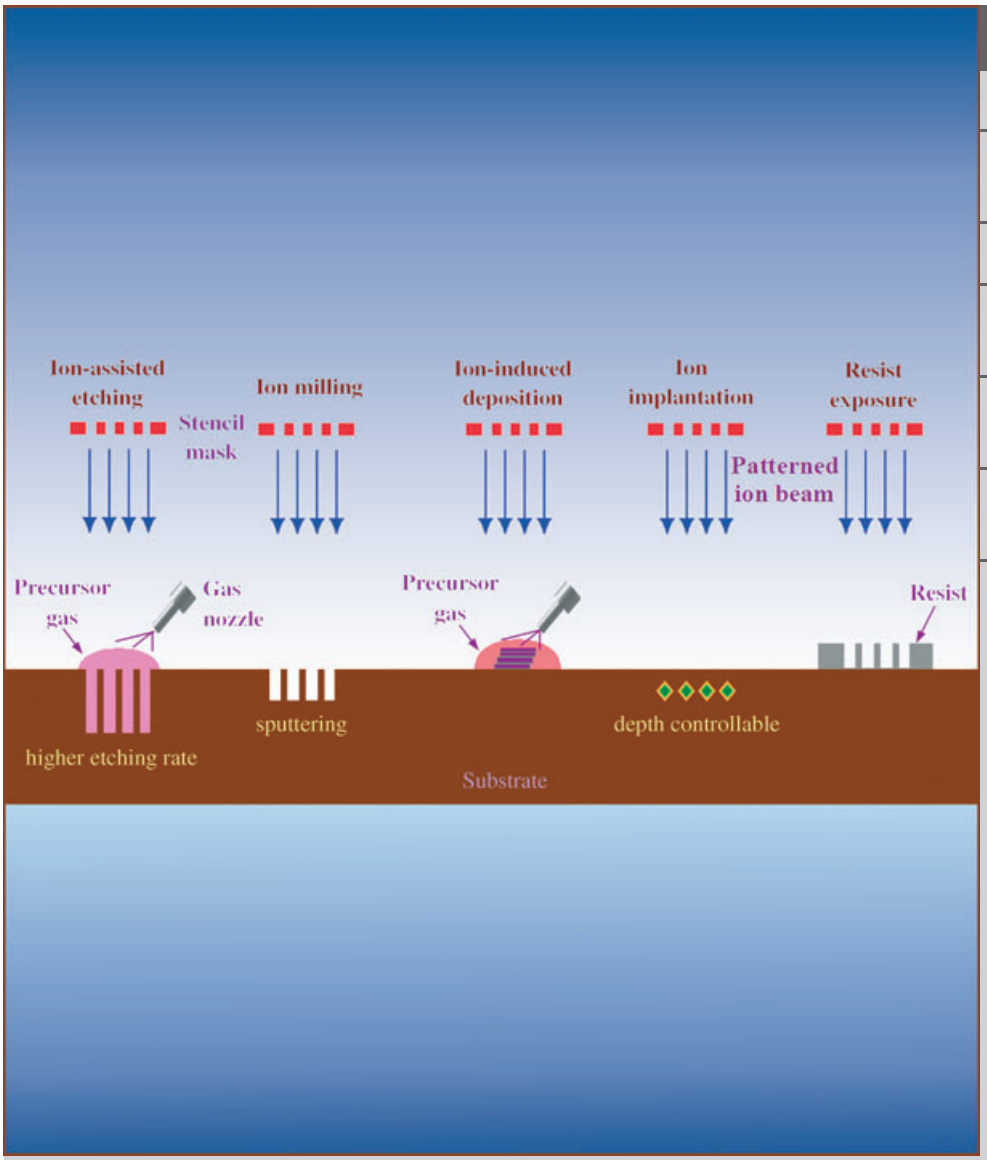

Ion projection lithography can be used to perform many different functions.

NANO MICRO small

From the Contents

Keywords:
- ion sources
- nanofabrication
- nanolithography
- nanostructures
- resists

DOI: 10.1002/smll.200500050

NANO MICRO small

Ion projection lithography (IPL) is an emerging technology and a major candidate for the next-generation lithography (NGL) designed to complement and supplement current optical lithographic techniques for future chip manufacturing. In this Review, the recent developments of IPL technology are examined with an emphasis on its ability to fabricate a wide variety of nanostructures for the semiconductor industry. Following an introduction of the uniqueness and strength of the technology, the basics of ion-source development and ion–target interactions with and without chemical enhancement are presented. The developments in equipment systems, masks, and resists are subsequently studied. The resolution of printed nanostructures and the corresponding throughput of the current system are assessed for NGL. Finally, concluding remarks are presented to summarize the strengths and weaknesses of the current technology and to suggest the scope for future improvement.

1. Introduction

In ion projection lithography (IPL), ions that are extracted from a source and collimated through a mask with the imaging pattern are accelerated through a series of electrostatic lenses that project the ions onto a wafer substrate, where the ions penetrate and modify the substrate materials. While passing through the lens system, the ions are accelerated from between tens of keV to hundreds of keV and thus, IPL can perform many different functions including resist exposure, direct material sputtering, and the initiation of chemical reactions for etching or deposition (as indicated in the frontispiece). In performing its major task, resist exposure, IPL is very similar to optical lithography (OL). Both use reduction optics to project an image onto the wafer, and stepping and repeating exposures are similarly performed with the use of a precisely controlled laser interferometer stage.

Basically, IPL has the capability to realize printed features at 50 nm resolution by using lightweight ions to expose a resist. A wide range of projection energy and ion species can be tailored to meet proper exposure or modification conditions of the material while at the same time causing no damage to the underlying materials or circuitries.[1,2] IPL also has a large depth of focus (up to ± 500 μm) and very short exposure times (less than 0.5 s). A variety of materials have been shown to work well with IPL and no major effort is needed to develop new resist materials. As a result, IPL has been selected as a major candidate for next-generation lithography (NGL). NGL refers to the post-optical lithography era and is designed to complement and supplement OL for future semiconductor manufacturing.

In addition to IPL, the candidates for NGL include extreme ultraviolet (EUV) lithography, electron projection lithography (EPL), direct-write e-beam lithography (EBL), and X-ray lithography (XRL). Also, imprinting lithography (IL) was added as an NGL candidate in the 2003 edition of the International Technology Roadmap for Semiconductors (ITRS) by SEMATECH.[3] Based on the current trend to produce ever-shrinking device sizes and increased processor speeds, it is expected that OL will become inadequate for making some critical elements by the end of this decade. This is when NGL technologies should take over production of these critical elements for state-of-the-art semiconductor devices. It is also expected that even after NGL becomes mature, OL will still be around and perform noncritical features. As such, NGL would coexist with OL for many more years and should be seamlessly implemented into the manufacturing lines built for OL.

Since the worldwide market for semiconductor products is huge (US$ 166 billion in 2003 according to the Semiconductor Industry Association), NGL technologies are all competing for a share of the next paradigm shift in lithography techniques. All of these technologies also have their own particular weaknesses. IPL certainly is not perfect, but it offers several advantages for semiconductor manufacturers. For example, XRL is too expensive and has a shorter lifetime than IPL. The e-beam technology is too slow and has far more potential for pitfalls than IPL. The optics for EUV are still problematic and have a relatively shorter lifetime than IPL. It is inevitable that all these NGL technologies have to make room for an alternative and complementary technology such as IPL.[4]

A shift by the semiconductor industry to any NGL technology would require the introduction of a new infrastructure of tools, materials, and processing techniques, the re-

[*] A. A. Tseng
Department of Mechanical and Aerospace Engineering
Arizona State University, Tempe, AZ 85287-6106 (USA)
Fax: (+1) 480-965-1384
E-mail: ampere.tseng@asu.edu

 DOI: 10.1002/smll.200500050

search and development costs of which would be enormous. A review article on IPL should provide the necessary information for making a good judgment in the selection of a NGL technique. As a result, the purpose of this Review is to assess the technical capabilities of IPL through an overview of its recent technical advances, especially the strength and weakness of the lithographic equipment already developed, as well as the resolution of the nanostructures made by the equipment. The ability to make a high-resolution structure is the most important and basic criteria in judging the suitability of NGL. At the present stage, to be competitive, any vital NGL candidate should have the ability to make nanoscale structures. Here, a nanoscale structure or nanostructure can act as a component, device, or system, having a feature size in the range from 0.1 to 100 nm.

In this Review, the current developments in the lithographic capabilities of IPL, including ion sources, equipment, masks, and resists are first assessed. To illustrate the versatility and advancement of these lithographic capabilities, a wide variety of nanostructures made by different exposures and trial conditions are subsequently examined with an emphasis on the resulted resolution and equipment throughput. Finally, a summary of the current progress and the scope recommended for future developments are provided to conclude the present study.

2. Ions and Interactions

Ions are particles with net electrical charges, which usually are atoms lacking one or more orbiting electrons. Therefore, they can be steered by electric or magnetic fields. In IPL, ions are collimated into a beam that passes through a stencil mask and is projected onto the substrate using electromagnetic lens systems. In this section, the characteristics and sources of ions as well as their interactions with other materials and chemicals are discussed and analyzed.

Ampere A. Tseng is a Professor at Arizona State University. He received his PhD in mechanical engineering from the Georgia Institute of Technology in 1978, and has published more than 200 peer-reviewed articles, edited more than ten technical books, and is the holder of ten US patents. He was a recipient of the Superior Performance Award and ASU Faculty Award (1999–2000). He chaired the ASME Materials Division in 1991–92 and was elected as an ASME Fellow in 1995. He also chaired the NSF Workshop on Manufacturing MEMS (2000) and co-chaired the International Conference of Transport Phenomena in Processing (1992) and the USA–China Workshop on Advanced Machine Tool Research (1999).

2.1. Characteristics of Ions

One of the most important features of IPL is that its ions have extremely small particle wavelengths (for instance, the de Broglie wavelength of 100 keV He^+ ions is just 5×10^{-5} nm), whereas photon-based OL or EUV lithography is operated at the diffraction-limited resolution at which the shortest wavelength currently considered is on the order of 10 nm in the EUV region. Certainly, charged-particle- (including ion-) based optical resolution is limited by lens aberrations. In general, for particle-based optics, one requires that the diffraction-limited resolution should be one tenth of the minimum feature size to be printed.

Moreover, ions possess advantages over other high-energy particles used in nanofabrication. For example, when compared to electrons, ions are much heavier and can strike with greater energy at relatively shorter wavelengths to directly transfer patterns onto hard materials (such as semiconductors, metals, or ceramics) without major forward- and back-scattering. Thus the feature size of the patterns is largely dictated by the beam size and the interaction of the beam with the target material. On the other hand, electrons or photons can mainly be applied for writing on soft materials (such as polymers or resists) and the corresponding feature sizes are determined by the proximity of the back-scattered electrons or wave diffraction limits. Moreover, the lateral exposure in an ion beam is very low, thereby exposing only the correct areas and writing very narrow lines in the substrate, which makes it more capable to directly fabricate nanostructures.[5–7]

2.2. Ion Sources and Beam Quality

The ion source is important because its properties affect many parameters involved in forming an ion beam as well as the interaction between the beam and substrates in fabrication. Two major types of ion sources, point and volume-plasma sources, have been developed to produce nanometer-resolution patterns. Normally, point sources are used to form a focused ion beam (FIB), in which a sharp dot image is focused directly on the substrate for direct writing. On the contrary, volume-plasma sources are used for IPL, in which a parallel ion beam is printed onto a substrate or resist through a mask with or without demagnification.

In general, the axial energy spread of the ion beam when coupled with the chromatic aberration in the ion optical column can lead to blurring in the printed pattern on the target. Recently, the multicusp volume-plasma source has replaced the duoplasmatron volume source for ion-projection printing because of its ability to provide a lower axial-energy spread of ions, which results in minimizing the chromatic aberration of the projected image. Also, the multicusp source can be used to produce large volumes of uniform, quiescent, and high-density plasmas with high gas and electrical efficiencies. The multicusp source is based on electron-impact ionization, in which the energy transferred to a gas molecule from an energetic electron exceeds the ionization energy by means of ionizing collisions. The electrons

NANO MICRO small

are energized through a gaseous discharge. Both the electrons and excited ions are accelerated by a dc field or rf power at a frequency of a few MHz (up to 13.56 MHz) and are confined by an imposed magnetic field. The multicusp source is generally used to produce hydrogen and helium ion beams. Other ion beams of Ne, Ar, and Xe can also be generated.

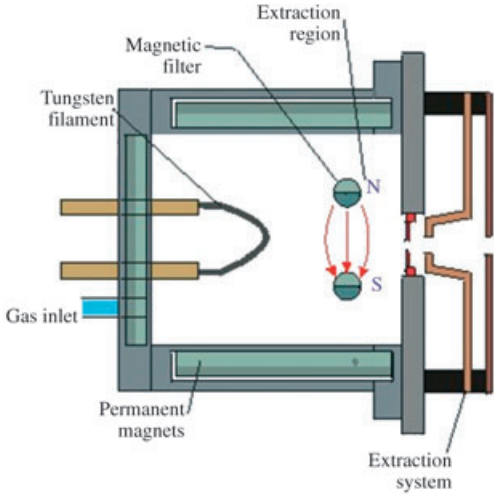

Figure 1. Multicusp ion source for dc discharge using a hot tungsten filament cathode with magnetic filters (courtesy of K. N. Leung of Lawrence Berkeley National Laboratory).

Figure 1 shows a schematic of a filament-discharge multicusp ion source. The external surface of the source chamber is surrounded by columns of permanent magnets (such as samarium–cobalt alloy magnets), which generate longitudinal line-cusp magnetic fields that can confine the primary ionizing electrons (plasma) efficiently. The magnets are placed around the cylindrical chamber and on the flange end, since an extraction system is frequently placed on the opposite (open) end. Such magnet placements result in an asymmetric distribution of the plasma potential inside the source that is crucial in controlling the axial or longitudinal energy spread.[8] The low-axial-energy ions are extracted from the open end of the chamber. Magnetic filters are used to reflect the high-energy electrons so that ion production occurs mainly in the region between the tungsten filament and the filter where there is high-density plasma and uniform plasma potential. The extracted ion beam, therefore, exhibits a low axial-energy spread that can be lower than 2 eV. On the other hand, the corresponding axial energy spread of a duoplasmatron ion source for a typical IPL system is in the range of 6 to 8 eV.[4]

Two current IPL systems are equipped with coaxial multicusp ion sources: one is known as ALG-1000 built by a consortium of industrial and research institutes in the US and Europe, the Advanced Lithography Group (ALG), while the other is the process development tool (PDT) supported by an international IPL development program called MEDEA. Using a specially designed extraction system, the PDT, for example, can extract a 5 keV He^+ beam to yield an axial-energy spread of as low as 0.6 eV. Consequently, this ion source can be expected to produce sharp features and achieve the 50 nm resolution target.[9] The light ions (H^+, H_2^+, H_3^+, He^+) are particularly suitable for projection printing because they have very little forward scattering and give off very small energy to the secondary electrons in the polymeric resist. More details of these two IPL tools will be elaborated later in Section 3.

Liquid-metal ion sources (LMISs) usually produce heavy and high-brightness ions that can be focused onto fine FIBs on the order of 10 nm with adequate current densities for direct writing. Normally, LMISs are not used for IPL and thus, are not elaborated here further. A good introduction on this subject can be found in other review articles.[7,10]

2.3. The Ion–Target Interaction

When an energetic ion collides with a target solid, it encounters numerous elastic and inelastic collisions with the atoms and electrons in the solid, which leads to different electronic and atomic interactions. Depending on the amount of ion energy, many interaction events, such as backscattering, sputtering, implantation, and nuclear reaction occur (as shown schematically in Figure 2). Some of the interactions are not completely separable and may lead to unwanted side effects that need to be understood and avoided for a specific application.

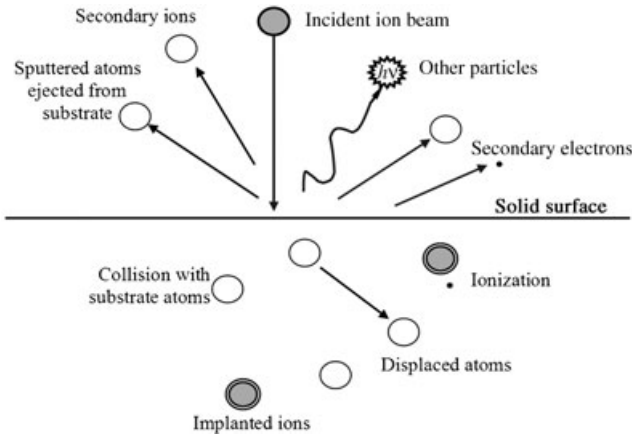

Figure 2. A schematic that shows the interactions that occur between ions and a target solid.

2.3.1. Elastic Interactions

If the incident ion is at a relatively low energy, it can be backscattered by an atom or a group of atoms in the target solid through an energy or momentum exchange between the ion and the atom (or atoms). The energy exchange or backscattering can result in a deflection of the ion from the incident path to a new trajectory. Also, if the associated ion

momentum is sufficiently large, an atomic dislocation can occur, in which a surface atom in the solid lattice can be dislodged from a weakly bonded position to a more strongly bonded one. Ions with greater energies can cause internal dislocations in the bulk of the target solid.

If the energy (or momentum) of the incoming ion is even higher, the collision can transfer enough momentum to entirely free one or more atoms, which are ejected from the solid as a result. This interaction is called sputtering and is the governing effect in an ion-milling process. The number of atoms that are ejected is called the sputter yield and is a measure of the efficiency of material removal. A small portion of these ejected atoms can leave as either positively or negatively charged ions, which are also known as secondary ions, and can be used for material analysis as discussed later. The yield is normally in the range of 1 to 50 atoms per ion and is a function of many variables, including the mass of the ion and target atom, ion energy, ion incident angle, target temperature, and ion flux. There is a threshold for sputtering to occur. At a point above the threshold, the sputtering yield rises to a maximum and eventually decreases at a relatively high energy as the ion penetrates into the solid and cannot reach the surface (ion implantation occurs). As a result, the proper energy for sputtering is between 10 to 100 keV for most ion species used. Because the sputtering depends solely on momentum transfer to remove the atoms, it is a purely physical process and, therefore, is also called physical ion etching.

As mentioned earlier, as the ion energy increases further, the ion penetrates into the solid and ion implantation occurs. The ion loses energy to the atoms and electrons in the solid and becomes trapped inside the lattice. The lost energy can also cause the atoms or nuclei in the solid to be displaced from their normal lattice sites. The trapped ions or replaced atoms can alter the properties of the solid. The semiconductor property change by doping is one of the most common examples of ion implantation. Normally, the depth of penetration decreases as the ion mass or the solid density increases.

Most of the above-discussed interactions, including scattering, sputtering, and implantation, involve momentum (or energy) exchange between the ion and the atom, and can be described by two-body elastic collisions. This type of interaction is often called an elastic interaction and can lead to the displacement of lattice atoms, sputtering, and the formation of defects.[11]

2.3.2. Inelastic Interactions

The incident ions also interact with the target's electrons, which can lead to useful signals for material analyses. In general, the interactions of the ion with the electrons do not cause any appreciable scattering of the incident ion because the momentum transfer is relatively small. However, the interactions create excitation and ionization of electron shells of both the incident and target atoms. If this excitation occurs near the surface, it results in the emission of secondary particles (electrons and ions), optical photons, and characteristic X-rays. This type of interaction involves different forms of energy or particles and is termed as an inelastic interaction (as opposed to the elastic interactions described earlier). The emission can be strong enough to be detected without excessive noise and thus is used as a signal to create high-magnification images of the target solid.

The technique of detecting the low-energy secondary electrons and/or secondary ions to determine the morphology or chemical composition of the target solid is called scanning ion microscopy (SIM). SIM is very similar to scanning electron microscopy (SEM). In both cases, charged particles are focused onto the surface of the target and rastered across it. SIM does not enjoy the popularity of SEM because the spot characteristics of ion beams are poorer than those of high-quality SEM. On the other hand, by supplying a broad low-energy electron beam to neutralize the targets or to eliminate the charge build-up, an SIM can be used for imaging a highly insulating target without a conducting surface coating, as would be required in an SEM.[10]

Furthermore, if the direction of the ion beam is aligned with a plane or axis of a crystal, ions travel through the crystal with less energy loss (lower collision loss) and result in a lower sputtering yield. This phenomenon is called channeling and has a profound effect on the secondary ion and electron yields. It has also been used in the development of masks for IPL. By differentiating the secondary particle yields with and without channeling, SIM can provide strong contrast images of crystallography for studying the local differences in a crystal. Also, SIM can supply more information about the chemical nature of the target surface, since low-energy electrons are sensitive to the work function of the surface. Similarly, SIM is also used for high-resolution surface analysis by detecting the secondary ions. Since the mechanisms to create the secondary electrons and secondary ions are different, the contrast obtained from each technique can provide much more information on the surface and amorphous characterizations.

The secondary ions can also be created by the incident ions through elastic nuclear collisions. The technique of detecting these secondary particles to provide different aspects of the examined target solid is called secondary ion mass spectroscopy (SIMS). Since the energy of a sputtered ion is relatively low and its range is very short, SIMS is extremely surface sensitive and provides real-time high-resolution images of the target material. Secondary ions originating from elastic nuclear collisions are somewhat difficult to distinguish from those created by inelastic atomic excitation and ionization. In fact, a typical SIMS probe uses the secondary ions generated by both elastic and inelastic interactions to perform the analysis. Typically, the ion energy used for SIMS and SIM is in the range of tens of keV, where the emitted secondary electrons have an energy distribution peak of a few eV and the secondary ions may have many keV of energy. Since SIMS or SIM works by analyzing material removed from the target by sputtering, it can be conveniently used in parallel with the FIB sputtering or milling processes. On the other hand, the fact that sputtering is a destructive process has also limited the applications of SIMS and SIM. The resolution for a modern SIMS or SIM apparatus can be as small as 20 nm.[12]

NANO MICRO small

In higher-energy collisions between the ion and the electrons, an electron can be ejected from an inner shell. Subsequently, the electrons in other shells rearrange themselves with the emission of a quantum of energy (X-ray), which is characteristic of the target atom. This X-ray signal can be used to quantify the chemical composition of the target solid with high accuracy and sensitivity. Detection of these X-rays can be accomplished by an energy- or a wavelength-dispersive spectrometer. For an ion energy increasing to MeV levels, interactions with a target solid can permit more analytical and imaging abilities. For example, techniques such as proton-induced X-ray emission (PIXE), proton-induced gamma-ray emission (PIGE), nuclear reaction analysis (NRA), and ionoluminescence have been developed to use the excited X-rays, excited γ-rays, outgoing nuclear reaction particles, and visible and infrared emissions, from the target materials, respectively. Many of these techniques can be combined with channeling to study the lattice location of species (channeling contrast microscopy). The use of ion beams for imaging or analyses is helpful, but is not directly related to IPL. Consequently, this subject will not be discussed any further.

At ultrahigh energies, normally much higher than 1 MeV, nuclear reactions may occur and the ion can inflict large-scale damage to the target solid. Practically, this level of ion energy is beyond the useful range for nanofabrication and will not be discussed here. Some recent developments in this subject, especially in heavy-ion reactions, may be found in the publication by Choudhury and Kicinska-Habior et al.[13,14]

2.4. Chemical Reactions

In addition to elastic and inelastic interactions with the target substrate, the energy of incident ions in the presence of a reactive gas can also lead to chemical reactions in the form of either ion-assisted etching (IAE) or ion-induced deposition (IID).

In IAE, the ion beam causes the precursor gas to react with the substrate material to form volatile products that can be easily removed by the pump system at rates much higher than sputtering alone. To have a better control of the etched dimension, the precursor gas should not react with the target substrate without the ion beam energy. The frequently used gases include halides (Br_2, Cl_2, I_2, XeF_2) for etching certain metals and insulators, and H_2O for carbon-based materials.

In IID, the ion beam causes the molecules of the precursor gas to dissociate and leave the desired reaction products on the target surface or the outermost layer of the deposited structure, while the volatile reaction products desorbed from the surface are removed through a vacuum pumping system. The precursor gases for metal deposition are normally organometallic. Insulators or polymeric materials can also be deposited by different gas mixtures. Although IID is based on a similar principle to that of chemical vapor deposition (CVD) used in the semiconductor industry, it has a better resolution with a lower deposition rate, which is especially appropriate for nanofabrication. Since the incident ions simultaneously sputter the target, the ion energy is normally controlled at less than 30 keV; otherwise, the sputtering rate can significantly diminish the deposition rate.

Within the focus of this Review, ions with moderate energy levels, typically in the range of 20 eV to 200 keV, are the main interest because at this range, the ions can be effectively used for IPL. The associated interactions, especially sputtering, implantation, and ion-aided chemical reactions, will be discussed separately with a focus on their specific fabrication techniques and nanoscale applications.

3. IPL Systems

In an IPL system, a collimated beam of ions passes through a mask and the ion beam is accelerated by an electrostatic lens to create a demagnified image of the mask on the wafer. The wafer is stepped chip by chip. It is not difficult for IPL to achieve the desired ion energy ($\approx$100 keV). In fact, most of the ion implanters currently used by the semiconductor industry can deliver a small-scale collimated beam of ions at this energy level. However, in IPL, it is a challenge to deliver a big enough exposure area, especially larger than 1 cm^2, at desirable energy levels with minimum energy spreads (less than a few eV). Many efforts that have been devoted to the enhancement of the exposure or projection area and other IPL-related technologies are discussed below.

3.1. IPLM and ALPHA

The first practical IPL tool, called the ion projection lithography machine (IPLM), was developed and has evolved through the efforts of a group of scientists and engineers at Ionen Mikrofabrikations Systeme GmbH (IMS), in Vienna, Austria. The IPLM-01 was the first prototype which, after being tuned up, became the IPLM-02 in 1988. This tool is still in use for performing research and prototype testing; some results from this tool are described in Section 4. IPLM uses 5$\times$ or 10$\times$ demagnifying ion-optics for the reduction printing of open stencil masks having a sub-100 nm resolution, as reported by Stengl et al.[15]

Figure 3 shows the trajectories of ions through the IPLM system. Ions are extracted from a source resulting in a divergent ion beam, which illuminates the mask with an energy of about 5 keV. The extracted ions are H, He, N, Ne, Ar, or Xe. The immersion lens accelerates the ions passing through the mask opening to a final energy of 60–90 keV or higher. The tool is equipped with a stable duoplasmatron ion source enabling a current density of 10 $\mu A\,cm^{-2}$. A preprojective lens octupole permits an electrostatic shift of the ion image in the x and y directions, and a solenoid at this site enables a rotation of the ion image through the action of the axial magnetic field. Furthermore, the scale of the projected ion image can be adjusted electronically within plus or minus 3 %. The IPL technique combines lithography with

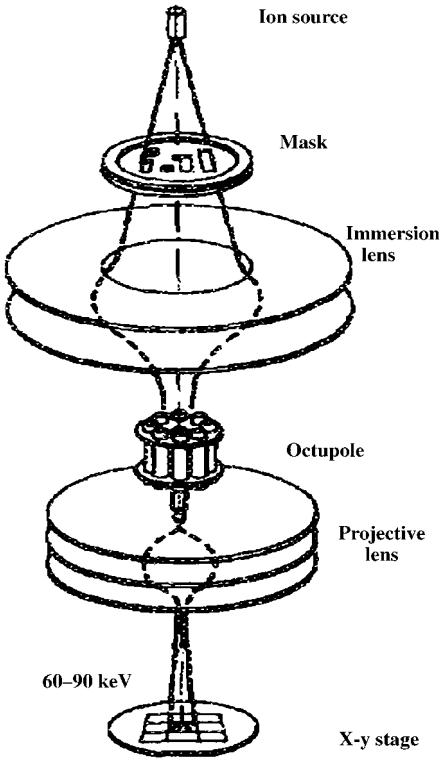

Figure 3. A schematic representation of the IPLM-2 lithographic system.

a direct sub-100 nm technique for ion-beam modification of materials.[16]

The next tool developed by IMS was the ALPHA-10X in 1990. This was an improvement over the IPLM-02 and was horizontally built. In order to increase the useable field size, the ALPHA machine reduction was changed from 10× to 5×, thereby increasing the field to $8\times8\,mm^2$ in 1991. With the ALPHA-5X, a total distortion of 150 nm was realized. This was in perfect agreement with the IMS ion-optical simulations and calculations.[1] Efforts to develop these two IPL tools by IMS demonstrated that IPL is a viable technology for future chip manufacture.

3.2. ALG

In 1992, the Advanced Lithography Group (ALG), a consortium of industry and university institutes in the US and Europe, was formed with a goal to produce an IPL tool, ALG-1000, for projecting patterns in a stencil mask onto a wafer substrate with a resolution less than 180 nm.[17–18] To reach this goal, special low-distortion ion optics were developed by IMS for exposing $20\times20\,mm^2$ fields at a 3× reduction. The ion source adopted by ALG-1000, designed by the Lawrence Berkeley National Laboratory (LBNL), is a 10-cm-diameter multicusp source, similar to that shown in Figure 1. The source can deliver a H^+ or He^+ beam with a useful beam current of 20 μA and an energy spread of less than 3 eV in order to limit the effect of chromatic aberration to below 25 nm. The ALG system utilizes off-axis wafer alignment, and a precision *x*–*y* stage controlled by a laser interferometer. The Einzel lens can project an ion image of the stencil mask onto the wafer substrate with better than 2 mrad telecentricity. Demonstrated IPL performance has shown less than 15 nm distortions over a $20\times20\,mm^2$ field and has indicated even larger fields being possible. Experiments have demonstrated that 100-nm-wide lines can be obtained in a Ray PN resist over an $8\times8\,mm^2$ field by using H^+ ions at 55 keV. On the other hand, the same experiment with a duoplasmatron source could only resolve 180-nm-wide lines.[16] At the end of the last century, through a contract with the US Defense Advanced Research Projects Agency (DARPA), the ALG-1000 was upgraded to ALG-1001 with all the necessary hardware and software as well as the ancillaries to make the ALG a production-ready tool and was specifically used to demonstrate overlay registration. Further refinement of the tool has been considered since.

3.3. PDT/MEDEA

In 1997, a new international consortium led by Infineon and Sematech, called MEDEA, was formed to build an IPL system known as the process development tool (PDT) for testing the virtual source size, energy spread, homogeneity, total extract current, and lifetime of the source. Major efforts have been dedicated to build on the previous ALG work and to implement a new multielectrode configuration to achieve a 50 nm resolution with an enhanced field size and a reduced column length.[19] A 4× reduction ion optics system has been developed for PDT, in which a printing area of $12.5\times12.5\,mm^2$ is designed to be patterned on to the wafer. To obtain a full image of the whole wafer area, each printing area is stitched one-by-one via synchronization of the beam and wafer moments.[20] The coaxial multicusp ion source used in PDT is also developed by LBNL, and has a very low energy spread at 1 eV FWHM (full-width at half-maximum) level. Multielectrode electrostatic-ion-optics has been used as the diverging electrostatic lens while an online diagnostic system and field-composable lens are used to compensate for mechanical manufacturing inaccuracies.

The PDT is the most recent tool developed by IMS. Both the PDT and ALG technologies can be categorized as second-generation IPL systems. As shown in Figure 4, the multicusp ion source of the PDT is equipped with a coaxial Wien (ExB) mass filter and passes through a multielectrode electrostatic ion-optics stage to condense the ions into a nearly telecentric ion beam of 115 mm in diameter (current size in PDT technology) to illuminate the stencil mask.[43] After passing through the stencil mask, the ion beamlets are further accelerated to energies in the 70–150 keV range, and then demagnified into a parallel beam whose image is focused at the wafer. Meanwhile, a pattern lock system monitors the positions of 12 reference beamlets as they travel through the ion-optical system. Diagnostic elements are provided to measure the energy spread, beam uniformity, and distortion. The uniformity of the current density can be controlled within 3% of the current PDT system. By system op-

NANO MICRO small

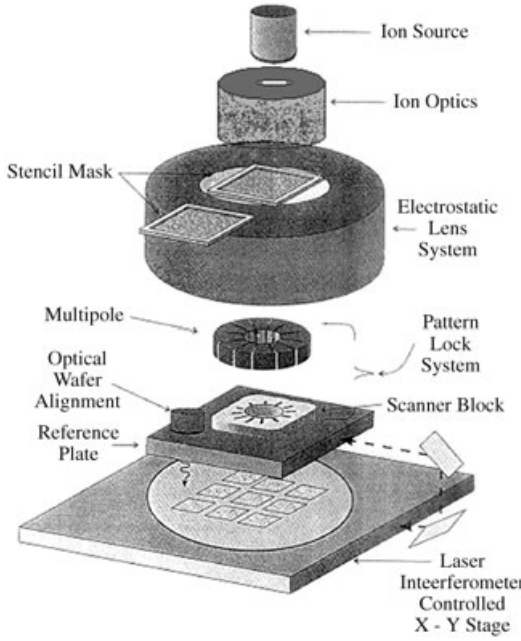

Figure 4. A schematic representation of the PDT/MEDEA lithographic system.

timization, it is expected that the uniformity can be achieved within 1%.

3.4. MMRL

Maskless or multibeam designs have also been considered for IPL. Ando and Muray[21] did a preliminary study of a multibeam IPL system, in which the multiple beams are created by a screen lens. The screen lens consists of an array of holes in a planar metal electrode and is used in conjunction with a single-object aperture, which is illuminated by a single ion beam. This object aperture is then demagnified by every hole in the screen lens, simultaneously forming multiple images of the object. However, all beamlets have to be deflected and blanked in synchronism and only one pattern can be written by a single beamlet. Later, Berry et al.[22] proposed a maskless system that uses an ion beam to illuminate a "blanking aperture array" and 200× reduction optics to expose the wafer in a scanning mode. This concept offers the advantage of using a single source and of realizing a 25 nm spot size at the wafer with $5 \times 5\ \mu m^2$ aperture dimensions. There are no mobile parts in the optics, that is, the only moving part in the system is a high-speed wafer stage.

By implementing the above multibeam and maskless concepts with some modifications, LBNL has developed a maskless IPL system, which is known as maskless microion-beam reduction lithography (MMRL), as shown in Figure 5. As reported by Ngo et al.,[23] MMRL consists of a coaxial multicusp ion source, a multibeamlet pattern generator, and an all-electrostatic accelerator column. The pattern generator is used to create a lithographic pattern to eliminate the need for masks. During processing, each individual ion

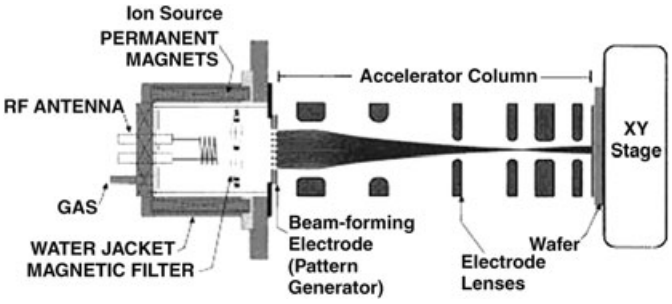

Figure 5. A schematic representation of the MMRL system, which uses a universal pattern generator to form a lithographic pattern (courtesy of K. N. Leung of Lawrence Berkeley National Laboratory).

beamlet can be switched on or off to form the lithographic pattern by biasing the extraction electrode with respect to the plasma electrode. Removing the use of stencil masks and the first stage, which is normally required by the other IPL systems (such as ALG and PDT), can eliminate the costs and efforts for mask development and fabrication, as well as providing great potential for reducing the equipment and operation costs. Jiang et al.[24] and Ngo et al.[23] have used nine 50 μm switchable apertures to generate beamlets with 10× reduction ion optics to demonstrate the proof-of-concept of MMRL, and concluded that the maskless system is a vital candidate for NGL.

However, the resolution of the pattern generated should be dictated by the number of beamlets. The ability to have a large number of beamlets is a major challenge for MMRL and a high-resolution image on the substrate is essential for the success of MMRL. No nano- or microscale structures have been directly printed by the pattern using the multiple beamlets. It is expected that a technology similar to the variable-shaped beam used in EBL will be developed for MMRL. In the variable-shaped beam technique, a reasonable number (initially, 36 to 64) of parallel ion beamlets have the ability to form several types of primitive shapes (mainly rectangles), and in every shot, only one of the shapes will be projected on the substrate with a certain level (8 to 10 times) of demagnification.[25] These primitive shapes are much smaller than the field sizes achieved in IPL. Thus, a few dozens of projected primitive shapes can then be stitched into the final pattern, equivalent to the field size (1 to 2 cm^2) in IPL. More complex shapes can also be achieved by splitting the rectangles before the exposure. MMRL incorporated with a variable-shaped beam system should be a more reasonable goal than developing a universal generator for the whole pattern in one shot. In this way, the shaped-beam system can increase the resolution by compromising the throughput achieved by the IPL system.

4. Projection Masks and Resists

The main challenge in IPL has been the projection mask because the absorption or transmission of ions is not similar to that of photons, in which the absorption or transmission

is determined by the band structure of the mask materials. Most materials, including the least dense resists, can highly absorb ions and cause scattering of an incident ion beam, as discussed earlier in Section 2.3. In fact, a collimated ion beam passing through a thin film or mask can emerge both diminished in number and in energy, and to some extent uncollimated. However, the difference in the energy loss rate in various materials is on the order of two, much smaller than that of the particles in X-ray or UV technologies. Therefore, the concept of using material difference for alternate areas of absorbing and transmitting is difficult for applications with IPL masks.

4.1. Stencil Masks

Most of the IPL systems use open stencil masks for pattern transformation as indicated by many investigators.[5,6,20] In the stencil mask, patterns are etched on the metal foils. This type of mask has excellent contrast because the ions are not affected by passing through the open hole before striking on the resist. However, not all of the features can be designed on a single stencil mask. A circle with middle fallout is a good example. Since there is no sublayer to hold the etched middle fallout, every feature in the etched pattern has to be connected to each other and no island or detached sections can be included in the pattern. This is also known as the "doughnut problem".

To cope with the geometric restriction in stencil masks, the detached features can be patterned on as split or complementary features, and it is the sum of these that produces the final intended features. In such an approach, the use of a "split" mass (two parts of the same device located on the same mask: an "A/B mask") or a complimentary mask (two or more separate masks, each containing a part of the device to be fabricated: "A + B masks") is required. Each of these techniques may also be used for layers that have extremely long runs of lines from one side of the device to the other. These layers can be split into what may look like dashed or segmented lines on one or each mask. When printed, these lines are joined together to reform the whole line pattern. A pattern lock system is then required to stitch or match these masks to print on the whole wafer.[1,20]

Furthermore, in order to avoid the use of complementary masks in disconnected geometries, continuous-membrane, single-crystal, channeling masks have been considered. The channeling mask benefits from the crystallographic channeling effect, that is, an increased range of ions incident along a crystal symmetry axis, as discussed in Section 2.3.2. Parma et al.[26] have studied a channeling mask that consists of a single-crystal silicon membrane about 10 μm thick that has been thinned to 0.6 μm, where transmission is desired. They found that ions with an incident energy of 180 keV can dissipate more than 50 keV of energy passing through the 0.61-μm-thick Si and also create some scattering. Their findings limit the resolution and the ultimate usefulness of the channeling mask, because the incident energy for most IPL systems is relatively low ($\approx$10 kV) and the likely increase in angular spread and energy spread due to scattering is not acceptable. Thus, further discussions will be limited to stencil masks.

4.2. Mask Fabrication

Single-crystal Si stencils appear to be popular because of their compatibility with the existing semiconductor processes and good control of mask stress. Typically, the fabrication process consists of three major steps: membrane etching, membrane implanting and framing, and stencil patterning.[27,28] The membrane is fabricated by anisotropic wet etching from the back side of a wafer (normally 500 μm thick), typically using KOH as the etchant and SiO_2 as the etching mask. A predefined p–n junction of 2 to 3 μm below the front surface is served as the etching stop. To prevent warping, the membrane is then prestressed by ion implantation (or doping) to certain tensile stresses, typically 10 MPa, which is somewhat lower than that of X-ray mask membranes. The membrane, with the perimeter of the original wafer serving as a frame, is bonded to a thicker, machined Si ring to ensure electrical conduction and thermal expansion compatibility. The oxide is then deposited on the front side of the membrane and patterned by standard EBL and reactive-ion etching (RIE). The 2 to 3 μm-thick Si membrane is then etched in a Br_2 RIE process with the oxide acting as an etching mask. This process yields reasonably good vertical sidewalls. Frequently, the back of the membrane is coated with carbon to protect it from ion bombardment and to increase the emissivity. The above process is similar to that of making piezoresistive pressure microsensors, except that the stencil mask can be as large as 200 mm and uses EBL for patterning.[29] A bonded stencil mask of 150 mm in diameter is shown in Figure 6a. The stencil pattern for structuring magnetic media is shown in Figure 6b, where the rectangular stencil openings are approximately 320 nm wide and 2000 nm long. The corresponding structures will be discussed in Section 5.2.

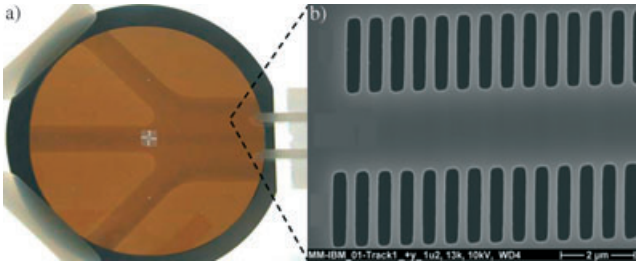

Figure 6. Silicon stencil mask fabricated by EBL for the PDT system: a) The whole mask (150 mm in diameter); b) stencil pattern for a resolution test (after Loeschner et al.[33]).

Recently, Letzkus et al.[30] developed a stencil mask with a thickness and diameter of 3 μm and 126 mm, respectively, for a PDT demonstration. They fabricated the mask on a silicon-on-insulator (SOI) wafer, in which the insulator layer is used as the etching stop, so that a predefined p–n junction is no longer required. Also, a deep RIE technique is adopted

NANO MICRO small

instead of regular RIE. In comparison with regular RIE, deep RIE relies on a high-density plasma and an alternating process of etching to provide better control of the steepness of etched vertical sidewalls and a higher trench aspect ratio.[29] The silicon membrane is also coated with a 500-nm-thick carbon protection layer to ensure adequate mask life. The mask developed by Letzkus et al.[30] is an overlay test mask and also consists of resolution test patterns (dense and isolated features). A mask containing an array of I-marks with a 400 nm linewidth for the resolution test is shown in Figure 7a (the printed structures will be presented later). After the mask is fabricated, other tasks including inspection, repairing, and cleaning should also be performed before installation.

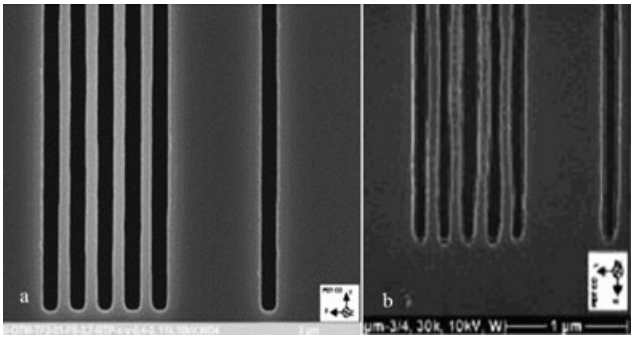

Figure 7. Mask-to-wafer transfer by PDT: a) SEM image of 400-nm-resolution patterns of an overlay test mask; b) 100 nm line-space pattern of demagnified mask contours printed in 240-nm-thick Shipley XP9946-D resist exposed by 37.5 keV He^+ ions at a dose of 1.35 $\mu C\,cm^{-2}$ (after Kaesmaier et al.[20] and Loeschner et al.[43]).

4.3. Mask Distortion

The mask in IPL is demagnified, so that the features on the mask are larger than those on the wafer, which makes the mask easier to fabricate from the point of view of resolution. However, this advantage has to be traded against the difficulties of making a larger-area membrane mask. So far, machines have been built with demagnification from 10:1 to 3:1. For 4× reduction optics, the masks made have a central area, for example, of 200 mm diameter, thinned to a membrane 2 to 3 μm thick, yielding a $50 \times 50\,mm^2$ image in the wafer. For such a large mask, the stencil membrane has to be under significant tensile stress in order to remain flat and prevent out-of-plane distortion, as well as to counterbalance the effect of gravity. Normally, a stress level on the order of 10 MPa is enough to ensure the flatness of the mask membranes.[6] Displacement and deformation by this level of stresses has to be compensated in the mask design stage, and the amount of compensation can be estimated by measurement[31] or numerical modeling.[32]

However, higher membrane stresses are undesirable because the stress relief produced by fabricating a pattern of openings in the stencil mask will cause in-plane distortions. If a pattern of holes is cut in a given area of the mask, the stress relief can cause lateral displacements in the non-cut areas of the mask. This will translate into a placement error in the features exposed on to the wafer. For some simple geometries, the local displacements in an Si membrane at a stretch stress of 10 MPa are approximately 0.5% of the opening's size. Thus, if the placement error is to be kept below 1 nm, the opening of the mask must be kept below 200 nm. For larger openings, compensation is needed, as mentioned earlier.[20] Mask distortion can also be reduced by introducing a perforated ring around the perimeter of the mask, as illustrated by Loeschner et al.[33] Certainly, reducing the initial membrane stress or using high-modulus materials can also alleviate the problems of distortion. Roughly speaking, the displacement is inversely proportional to the elastic modulus of the membrane material. The initial tensile stress can be introduced or adjusted by controlling the implantation and annealing conditions during fabrication.

Another major source of mask distortion is thermal expansion due to mask heating. The membrane is typically irradiated with a 10 keV ion beam at a current of $0.3\,\mu A\,cm^{-2}$ with a corresponding energy of $0.3\,mW\,cm^{-2}$. Since the mask is operated in a vacuum, no convection occurs. Heat is lost only by conduction to the rim and by radiation. Thus, the temperature at the center of the membrane will be higher than at the edges. Again, this has been verified both by modeling and by measurement. A temperature difference of about 10°C between the edge and the center can result in an unacceptable, nonuniform radial distortion of about 200 nm. Reducing the temperature nonuniformity can be critical in the operation of IPL for nanofabrication. Several schemes have been developed to reduce the thermal distortion. As indicated by Riordon et al.,[34] a cooled cylinder can be placed around the mask, and can effectively cool the mask to more than 20°C below the ambient temperature. Also, as discussed by Torres et al.[35] and Braun et al.,[36] since the mask is cooled the same way as it is heated, namely by radiation, radiation cooling can be used to minimize the thermal distortions of the stencil masks at high irradiation intensity. Furthermore, using low-expansion materials can alleviate the thermal distortion, which, in general, is proportional to the thermal expansion coefficient of the mask materials and the feature size. Invar is a Fe–Ni alloy that has a very low thermal expansion coefficient, excellent durability, and good forming properties, which makes it a good candidate for making masks.[37] More systematic research is needed to quantify the distortion sources in order to select better mask materials and to provide guidelines for minimization or compensation.

4.4. Resists for IPL

The major function of IPL is to produce a precise dose and energy of ions in the substrate. The pattern transformation requested by NGL is normally accomplished by the use of a resist, namely, a radiation- (or ion-energy-) sensitive polymer film. Similar to photo- or electron resists, ion resists have positive and negative types, where the former uses ions to break the long molecular chain to make the exposed resist soluble, while the latter employs ions to produce

cross-linking between molecules to strengthen the exposed resist, thus making it more insoluble. The resist sensitivity is a measure of the minimum dose (in units of $\mu C\,cm^{-2}$) needed to achieve these changes (e.g., a positive resist becoming complete dissolved). The resist sensitivity using ions is normally two orders of magnitude lower than that with electrons. The main reason for this is that ions in the range of 1–200 keV lose most their energy in the resist (more precisely, energy loss due to collisions with other particles, see Section 2), while electrons in this range can penetrate through the thin resist and lose a small fraction of their energy in the resist (because of their size, the collision frequency of electrons with other particles is much lower than that of ions). As a result, high-sensitivity resists are not required, since the dose requirement to expose most organic resists is in the range from 5×10^{11} to 3×10^{13} ions cm^{-2} and this range of ion energy can be relatively easy to obtain in IPL. In addition, by adjusting the ion energy, the penetration depth can be conveniently matched to the desirable exposure depth of the resist. Thus, high-aspect-ratio structures can be relatively easily fabricated.

Since a variety of resists are appropriate for IPL, no major efforts have been dedicated to develop new resist materials. Poly(methyl methacrylate) (PMMA), G-line, I-Line, and deep-ultraviolet (DUV) resists with both positive and negative tones work well with IPL.[20,23] DUV chemical-amplified resists (CARs) and PMMA are the two most popular types of IPL resists and have the best combination of resolution, minor sensitivity, and etch resistivity. Other DUV resists appropriate for IPL include Hoechst's AZ series, Olin's HPR 506, and OCG's HPR and ARCH.[6,38] By applying the top surface imaging (TSI) principle and using Ga ion-beam exposure associated with silylation and oxygen dry etching, a diazonaphthoquinone (DNQ)/novolak-based resist pattern can be obtained at a size as small as 30 nm while maintaining a high aspect ratio of up to 15, as indicated by Arshak et al.[39] It should be noted that the vacuum system used in IPL may cause outgassing of resists. More discussions on ion resists can be found elsewhere.[38,40,41]

5. Nanostructures Printed by IPL

Two types of nanostructures can be printed by IPL. The first type are polymeric resists used as the masks for the subsequent etching or deposition for transferring patterns to the underneath substrate, similar to the photoresist used in OL. The other uses IPL to directly sputter features in or deposit features on to the substrate. Very often, the resist materials can also be adopted as functional components and no subsequent etching or deposition for pattern transferring is needed. In this section, both the polymeric resists and direct-printed structures are discussed.

5.1. Resist Patterning

For a resolution test, the stencil mask shown in Figure 6b was used to expose a 50-nm-thick CARL resist using a PDT with 45 keV He^+ ions at a dose of 2.0 $\mu C\,cm^{-2}$. The CARL resist, developed by Infineon Technologies (Germany) for thin-film imaging, requires an exposure time of a few seconds.[40] As expected, through the 4× reduction ion-optics of PDT, the 320-nm-wide slots in the mask printed about 80-nm-wide slot patterns in the resist, as shown in Figure 8a. In addition to this slot pattern, a pattern for a DRAM device test is also included in the same mask. The printed DRAM device image is shown in Figure 8b, and indicates that 60-nm-wide ribs and spaces can be obtained. Since both patterns are projected through a single mask, they can only be printed in the same resist at the same exposure conditions.[33]

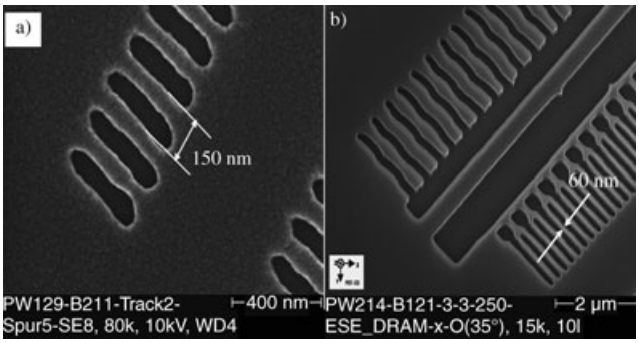

Figure 8. Exposure resolution test using 4× PDT with 45 keV He^+ ions at a dose of 2.0 $\mu C\,cm^{-2}$: a) SEM image of a 80-nm-wide slot array at a 150 nm period in 50-nm-thick Infineon CARL resist, using the stencil mask shown in Figure 6b; b) SEM image of a DRAM device test pattern with 60 nm ribs in 230-nm-thick Infineon CARL resist (after Loeschner et al.[33]).

The stencil mask fabricated on a SOI wafer shown in Figure 7a contains an array of overlay measurement marks and has been used for overlay tests. By a 4× reduction using PDT, one of the overlay I-marks with a 400 nm linewidth (Figure 7a) has been successfully used to print a 100-nm-wide I-mark pattern in a 240-nm-thick Shipley XP9946-D resist, as shown in Figure 7b.[20] A 37.5 keV He^+ ion beam at an exposure dose of 1.35 $\mu C\,cm^{-2}$ is used to project the I-mark pattern onto this Shipley DUV chemical-amplified resist, which exhibits a sensitivity of 0.8 $\mu C\,cm^{-2}$ for 37.5 keV He^+ ions.[42] This result and the resolution tests shown in Figure 8a and b have demonstrated that mask-to-wafer transfer for isolated and arrayed lines/spaces can be performed within the required accuracy. Also, as reported by Loeschner et al.,[43] some pattern collapse for 60 nm resist lines may be the limiting factor for determining the ultimate resolution of IPL.

Moreover, exposures have been performed using the IPLM-02 ion projector on a Shipley UVII HS resist.[41] A 3.5 keV He^+-ion beam is used and accelerated behind the mask to 75 keV. The resist used has been diluted so that a thinner resist of 180-nm thickness can be obtained. For an H^+-ion exposure of 75 keV, the resist sensitivity is 10^{12} ions cm^{-2}, which corresponds to 0.15 $\mu C\,cm^{-2}$. An open stencil mask with arrayed patterns fabricated on a SOI wafer was used for a resolution study. Figure 9a shows the

NANO MICRO small

stencil mask with a 650 nm linewidth, while through an 8.7 demagnification by ion optics, a pattern of 75-nm-wide lines and spaces is printed on the DUV resist without a pattern collapse, as shown in Figure 9b. As indicated in Figure 9,

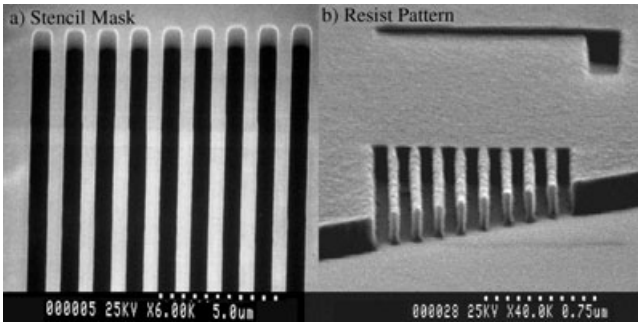

Figure 9. IPL resolution evaluation: a) SEM image of a stencil mask with 650-nm-wide lines and spaces; b) SEM image of a 75 nm line pattern printed by 8.7× reduction in 180-nm-thick Shipley DUV resist, exposed by 75 keV He^+ ions at a dose of 0.46 $\mu C\,cm^{-2}$ (courtesy of W. H. Bruenger, Fraunhofer Institute, Berlin).

the mask shows good edge quality, while in the exposed resist, no proximity effect is visible at the line ends in the exposed resist pattern, even though the resist has been removed by a second exposure of equal dose to allow the side view to be imaged by SEM. It is noteworthy that the higher dose used in the test can effectively reduce the edge roughness of the resist.

The IPLM-2 has also been used to assess the effect of the ion axial energy spread or beam quality on the printed structures. The multicusp ion source shown in Figure 1 can be equipped with a removable magnetic filter system, which can be used to provide a limited region of a transverse magnetic field that prevents the energetic electrons in the discharge chamber from crossing over into the extraction region. The plasma potential distribution in this case is more uniform, and results in a narrowed axial energy spread of approximately 2 eV for a 10-cm-diameter by 10-cm-long filament discharge source.[8] Without the planar magnetic filter system, the source in IPLM-2 is known to have an energy spread of approximately 12 eV, which is measured using a retarding-field energy analyzer. Figure 10

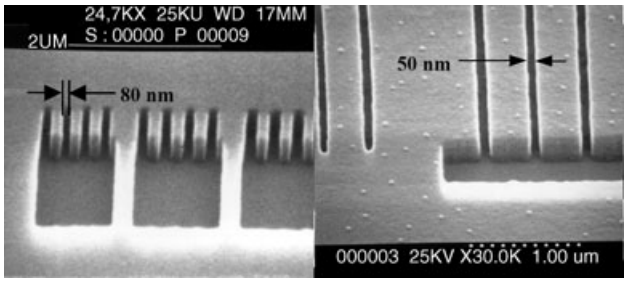

Figure 10. Resist nanostructures printed by IPML-2 (for assessing the effect of ion axial energy spread) using an ion source with a 12 eV axial energy spread (left), and a 2 eV axial energy spread (right; after Lee et al.[8]).

shows the exposure results for a 390-nm-thick DUV resist (Shipley UVII HS) using 74 keV H^+ ions with an exposure dose of 0.3 $\mu C\,cm^{-2}$. At an 8.4 ion-optical reduction with a normal energy spread of 12 eV, the printed structure with a 300 ms exposure time has a line space of 80 nm, as shown in Figure 10a, while by using the planar magnetic filter (having an energy spread of 2 eV), the corresponding line space or resolution improves to 50 nm with an exposure time of 800 ms, as shown in Figure 10b. The aspect ratio of the printed line trench also increases from less than 3:1 to greater than 4:1 with the magnetic filter. The study of Lee et al.[8] demonstrates that the lower the energy spread, the better the resolution and higher the aspect ratio of the printed structures.

5.2. Direct (Resistless) Printed Nanostructures

Ions have the unique feature of directly modifying a wide range of materials without the need of a resist. In IPL, a whole surface area can be treated in parallel and can be patterned into a substrate in a single-step process that should be much faster than the series process or direct writing using FIB. IPL has been used for the resistless patterning of semiconductors (Si, GaAs, poly-Si), insulating layers (SiO_2, Si_3N_4), and metals (Al, Ni, Mo, Au) in addition to patterning organic thin films and resists. Under many conditions, it is desirable to avoid the use of a resist. For instance, while making high-temperature superconductor nanostructures, undesirable chemical reactions can occur within the resist.

Brunger et al.[44] have used the IPLM-02 ion projector to perform direct milling on a 35-nm-thick Au film using an open stencil mask with 8.7-demagnification ion optics. To increase the milling rate, the light ions normally provided by the multicusp ion source used in IPLM-02 are replaced by the heavier Xe^+ species without any change in emission stability or uniformity. Figure 11a shows an array of line patterns milled with a dose of 2×10^{15} Xe^+ ions cm^{-2} at 75 keV having the smallest linewidth of 130 nm, while based on the profile measurement by white light interferometry shown in Figure 11b, the milling depth is 8 nm. The apparent roughness of the gold film is believed to be due to its grain structure.

IPL milling should be especially attractive for fabricating magnetic nanodots since other techniques, including OL,

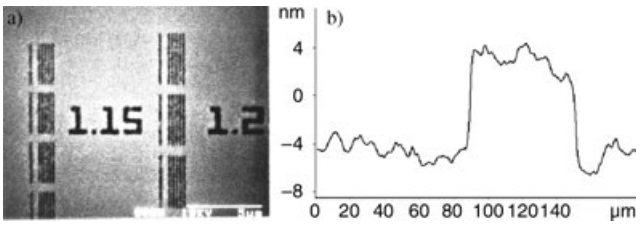

Figure 11. IPL milling with 2×10^{15} Xe^+ ions cm^{-2} at 75 keV in a polycrystalline Au film: a) SEM image of a milled line pattern with a minimum width of 130 nm; b) surface-depth profile of the milled pattern (courtesy of W. H. Bruenger, Fraunhofer Institute, Berlin).

EBL, and IL, have to use resist-based processes that are not preferable to keep the topography of a surface unchanged. This is extremely important for magnetic disks with a surface roughness of a few nanometers. Through a stencil mask, Dietzel et al.[45,46] used the IPLM-02 projector with a 3×10^{14} Xe^+ ions cm^{-2} dose at 73 keV to mill magnetic Co–Pt multilayers. Based on the magnetically altered areas measured by magnetic force microscopy (MFM), Dietzel et al.[45] reported that magnetic islands with an average diameter of less than 100 nm are formed. Also, atomic force microscopy (AFM) measurements indicated that the surface roughness of the topography after the IPL process is 1.1 nm (rms), which confirms that the topography change by IPL is negligible. Thus, IPL is acceptable for magnetic media applications. Earlier, Brunger et al.[44] also used the IPLM-02 projector to mill a magnetic FePt film using a 10^{16} He^+ ions cm^{-2} dose at 75 keV and reported that the averaged magnetic island size is 340 nm. By experimental evidence and numerical simulation, Dietzel et al.[45] and Brunger et al.[44,47] noticed that Xe^+ or Ar^+ are more effective by two orders of magnitude compared to He^+. Since the size limit of the magnetic dot is mainly controlled by the size of the open stencil mask holes, they also believe that based on the results obtained by Lee et al.[8] and with an appropriate mask design, IPLM-02 can make magnetic dots as small as 50 nm in diameter, which would result in a storage density better than 10 Gbit cm^{-2}.

Spiegel et al.[48] have used the IPLM-02 with Ar^+ ions to create desirable surface damage that can be used to initiate selective electroplating. The surface damage can significantly lower the Schottky barrier breakdown potential of semiconductors, and can be used to selectively porosify different semiconductors, as well as to deposit metals and semiconductors. The study also indicates that electroplating reactions can be selectively triggered on the surface previously damaged by ions. No mask is needed for electroplating. For copper electroplating, an electrolyte with the following composition was used: 0.05 M $CuSO_4$ + 0.5 M H_2SO_4 + 0.1 M benzotriazole (BTA). A potential of −1500 mV was applied for 18 s. Figure 12 shows the copper structures electroplated on the surface of a p-type Si(100) wafer with the damage caused by Ar^+ ions at an energy of 75 keV. A dose of 10^{13} ions cm^{-2} is delivered in 1 s. The structures resolved are on the order of 200 nm in diameter, however, both selectivity and sharpness still leave room for improvement. In order to prevent the formation of photogenerated charge carriers, the study was carried out in a black box, which also acted as a Faraday cage. Other metals, including Au and Ni, have also been electroplated using a similar process.

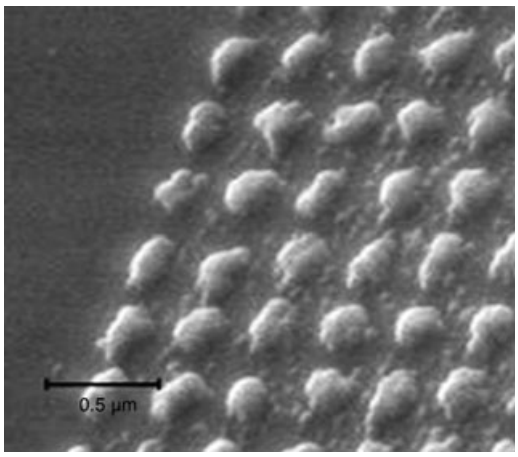

Figure 12. SEM image of Cu structures electroplated on a p-Si(100) wafer with exposure to 10^{13} Ar^+ ions cm^{-2} at 75 keV (after Spiegel et al.[48]).

The currently developed IPL techniques are not appropriate for ion implantation. PDT, ALG, and IPLM-02 all use light ions such as H^+ and He^+ for lithography, whereas for ion implantation or doping, the ability to handle other types of ions, especially, boron, phosphorus, and silicon, is essential. Also, with the current IPL systems, the stencil mask is placed on the low-energy side and the ions are accelerated behind the mask. Due to ion-optical reasons, ion-projection implantation requires the mask to be placed downstream from the accelerator. Consequently, no efforts have yet been reported to use PDT, ALG, or IPLM-02 for ion implantation.

Currently, for most industrial applications of ion implantation, ion beams equipped with either contact- or proximity-printing masks are used and have the capability to make implanted features near or within nanoscale arenas.[49,50] In fact, almost all modern CMOS devices are made by one or more implantation steps, but their masks are still patterned by the normal OL processes.[51] It should also be noted that both proximity and contact exposures have their limitations, especially as the exposure areas are limited to 1 cm^2. The angular dispersion makes it difficult to replicate patterns by means of proximity exposure. On the other hand, contact exposure can cause a decreased yield and reliability. As a result, ion implantation for making special nanodevices is mainly performed by non-projection processes.

6. Conclusions and Outlook

The recent progress of ion projection lithography (IPL) for nanofabrication has been examined with an emphasis on its ability to be a leading candidate for next-generation lithography (NGL). The key to IPL is the ability to operate a high-quality ion beam with an optimal beam size, current, and energy to make nanoscale patterns at low costs in large quantity. In general, IPL technology has been developing rapidly and advancements have been made in their resolution and precision. The critical feature sizes of the printed patterns can reach the level of 50 nm (e.g., the grooves or lines in Figure 10b), thus making IPL highly promising and a supplement to the current optical lithography (OL) techniques for future semiconductor manufacturing.

IPL has many advantages as compared to other NGL candidates. IPL is very similar to OL as both use reduction optics to project an image to the wafer. Step and repeat exposures are similarly performed with the use of a precisely controlled laser interferometer stage. It is expected that IPL has the advantages to be conveniently implemented into

NANO MICRO small

current OL lines at minimal cost. Also, the particles or ions used in IPL have extremely small particle wavelengths (e.g., the wavelength of 150 keV He^+ ions is about 10^{-4} nm). On the other hand, photon-based OL or EUV lithography is operated at the diffraction-limited resolution, where the shortest wavelength currently considered is on the order of 10 nm in the EUV region. Consequently, ion-based or IPL resolution is limited by lens aberrations. In general, for ion-based optics, one requires that the diffraction limited resolution should be one tenth of the minimum feature size to be printed. As a result, IPL has the capability to realize printed features well below the current state of the art, that is, 50 nm, by using lightweight ions.

The ability to use IPL for resistless or direct printing has been demonstrated. If this unique IPL capability is implemented, a number of steps in IPL can be eliminated and the entire lithographic process can be greatly simplified. However, one concern would be mask erosion. Although H^+ mask erosion is negligible, the erosion with heavier ions needed for semiconductor doping can be serious and can deteriorate the integrity of the mask. Other advantages include a large depth of focus (DOF) and small scattering in the resist (negligible diffraction or proximity effects). With negligible diffraction, the DOF can be as high as 1 mm for most light ions. The large DOF allows IPL to tolerate large field curvature and to produce high-aspect-ratio structures. A variety of existing resists are appropriate for IPL and there is no necessity to develop new resist materials for IPL. The associated exposure times for most ions are less than a fraction of one second. A wide range of ion species and energies can be selected for exact penetration depth into the resist.

Nevertheless, the superiority of any technology is often governed by many factors, which may be interplayed with one another; technical ability is only one of them. In IPL, the factors of competing technologies, resource allocations, and perceived or envisioned abilities could play a critical role in determining its future. As a result, despite impressive progress being achieved in IPL, there are heavily funded competing efforts and good advancement in other technologies. At this moment, the winner for NGL is still difficult to predict. Furthermore, since the disadvantages of using stencil masks, especially the complexity and precision requirement in applying the complementary masks, are rather overwhelming, it is believed that without major improvement of its mask system, IPL will have difficulties in being the sole or major lithographic technology for the future semiconductor industry. Consequently, research on new IPL-mask concepts and development for the channeling or complimentary masks should be encouraged. On the other hand, because of its low cost-of-ownership (that is, low anticipated total system cost and high throughput) and superiority in patterning the geometries without the need for complimentary masks, it is expected that IPL will at least play a major complementary role to supplement other mainstream processes and facilities.

Acknowledgements

The author gratefully acknowledges the support for this study by the US National Science Foundation under Grant Nos. DMI-0002466, CMS-0115828, and DMI-0423457.

[1] R. Mohondro, *Semiconductor Fabtech, Issue No. 3*, Henley Publishing, London, **1995**, pp. 177–183.
[2] L. L. Berry, *J. Vac. Sci. Technol. B* **1998**, *16*, 2444–2448.
[3] SEMATECH **2004**, "International Technology Roadmap for Semiconductors" in http://public.itrs.net/Files/2003ITRS/Home2003.htm.
[4] A. Heuberger, W. Brunger, *Microelectron. Eng.* **1996**, *34*, 39–50.
[5] U. S. Tandon, *Vacuum* **1992**, *43*, 241–251.
[6] J. Melngailis, A. A. Mondelli, I. L. Berry, R. Mohondro, *J. Vac. Sci. Technol. B* **1998**, *16*, 927–957.
[7] A. A. Tseng, *J. Micromech. Microeng.* **2004**, *14*, R15–R34.
[8] Y. Lee, K. N. Leung, M. D. Williams, W. H. Brunger, W. Fallmann, H. Loeschner, G. Stengl, *Proc. IEEE 1999 Particle Accelerator Conference*, IEEE, **1999**, pp. 2575–2577.
[9] H. Loeschner, E. J. Fantner, R. Korntner, E. Platzgummer, G. Stengl, M. Zeininger, R. Berger, W. H. Brunger, A. Dietzel, M.-I. Baraton, L. Merhari, J. E. E. Baglin, *Mater. Res. Soc. Symp. Proc.* **2002**, *739*, 3–12.
[10] J. Orloff, *Rev. Sci. Instrum.* **1993**, *64*, 1105–1130.
[11] I. Brodie, J. J. Muray, *The Physics of Micro/Nano-Fabrication*, Plenum, New York, **1992**.
[12] K. Kimura, K. Nakajima, H. Kobayashi, S. Miwa, K. Satori, *Appl. Surf. Sci.* **2003**, *203/204*, 418–422.
[13] R. K. Choudhury, *J. Phys.* **2001**, *57*, 585–600.
[14] M. Kicinska-Habior, Z. Trznadel, O, Kijewska, E. Wojcik, *Acta Phys. Pol. B* **2002**, *33*, 949–956.
[15] G. Stengl, H. Loeschner, M. Maurer, P. Wolf, *J. Vac. Sci. Technol. B* **1986**, *4*, 194–200.
[16] W. H. Brunger, H. Loeschner, G. Stengl, W. Fallmann, W. Finkelstein, J. Melngailis, *Microelectron. Eng.* **1995**, *27*, 323–326.
[17] W. Finkelstein, A. A. Mondelli, *Semicond. Int.* **1995**, *18*, 107–110.
[18] Y. Lee, R. A. Gough, W. B. Kunkel, K. N. Leung, L. T. Perkins, D. S. Pickard, L. Sun, J. Vujic, M. D. Williams, D. Wutte, A. A. Mondelli, G. Stengl, *Nucl. Instrum. Methods Phys. Res. Sect. A* **1997**, *385*, 204–208.
[19] G. Gross, R. Kaesmaier, *J. Vac. Sci. Technol. B* **1998**, *16*, 3150–3153.
[20] R. Kaesmaier, A. Ehrmann, H. Loschner, *Microelectron. Eng.* **2001**, *57–58*, 145–153.
[21] M. Ando, J. J. Muray, *J. Vac. Sci. Technol. B* **1988**, *6*, 2120–2123.
[22] L. L. Berry, A. A. Mondelli, J. Nichols, J. Melngailis, *J. Vac. Sci. Technol. B* **1997**, *15*, 2382–2386.
[23] V. V. Ngo, B. Akker, K. N. Leung, I. Noh, K. L. Scott, S. Wilde, *J. Vac. Sci. Technol. B* **2003**, *21*, 2297–2303.
[24] X. Jiang, Q. Ji, L. Ji, A. Chang, K. N. Leung, *J. Vac. Sci. Technol. B* **2003**, *21*, 2724–2727.
[25] A. A. Tseng, K. Chen, C. D. Chen, K. J. Ma, *IEEE Trans. Electron. Packag. Manuf.* **2003**, *26*, 141–149.
[26] E. J. Parma, R. R. Hart, J. L. Bartelt, *J. Vac. Sci. Technol. B* **1987**, *5*, 228–231.
[27] S. V. Pendharkar, J. C. Wolfe, H. R. Rampersad, Y. L. Chau, D. L. Licon, M. D. Morgan, W. E. Horne, R. C. Tiberio, J. N. Randall, *J. Vac. Sci. Technol. B* **1995**, *13*, 2588–2592.
[28] B. Volland, F. Shi, H. Heerlein, I. W. Rangelow, P. Hudek, I. Kostic, E. Cekan, H. Vonach, H. Loeschner, C. Horner, G. Stengl,

H. Buschbeck, M. Zeininger, A. Bleeker, J. Benschop, *J. Vac. Sci. Technol. B* **2000**, *18*, 3202 – 3206.
[29] G. T. A. Kovacs, *Micromachined Transducers Sourcebook*, McGraw-Hill, Boston, **1998**, pp. 252 – 254.
[30] F. Letzkus, J. Butschke, B. Höfflinger, M. Irmscher, C. Reuter, R. Springer, A. Ehrmann, J. Mathuni, *Microelectron. Eng.* **2000**, *53*, 609 – 612.
[31] J. L. Torres, J. C. Wolfe, P. Ruchhoeft, T. F. Kennedy, J. Podolski, K. Kragler, A. Ehrmann, R. Kaesmaier, H. Loeschner, *J. Vac. Sci. Technol. B* **2002**, *20*, 3095 – 3098.
[32] R. Tejeda, G. Frisque, R. Engelstad, E. Lovell, E. Haugeneder, H. Loeschner, *Microelectron. Eng.* **1999**, *46*, 485 – 488.
[33] H. Loeschner, G. Stengl, H. Buschbeck, A. Chalupka, G. Lammer, E. Platzgummer, H. Vonach, P. W. H. de Jager, R. Kaesmaier, A. Ehrmann, S. Hirscher, A. Wolter, A. Dietzel, R. Berger, H. Grimm, B. D. Terris, W. H. Bruenger, G. Gross, O. Fortagne, D. Adam, M. Böhm, H. Eichhorn, R. Springer, J. Butschke, F. Letzkus, P. Ruchhoeft, J. C. Wolfe, *J. Microlithogr. Microfabr. Microsyst.* **2003**, *2*, 34 – 48.
[34] J. Riordon, L. Didenko, J. Melngailis, *J. Vac. Sci. Technol. B* **1996**, *14*, 3900 – 3901.
[35] J. L. Torres, H. N. Nounu, J. R. Wasson, J. C. Wolfe, J. Lutz, E. Haugeneder, H. Loeschner, G. Stengl, R. Kaesmaier, *J. Vac. Sci. Technol. B* **2000**, *18*, 3207 – 3209.
[36] D. Braun, R. Gajic, F. Kuchar, R. Korntner, E. Haugeneder, H. Loeschner, J. Butschke, F. Letzkus, R. Springer, *J. Vac. Sci. Technol. B* **2003**, *21*, 123 – 126.
[37] A. A. Tseng, J. Muller, Y. H. Hahn, *Mater. Des.* **1996**, *17*, 89 – 96.
[38] W. H. Brunger, M. Torkler, M. Weiss, H. Loeschner, K. Leung, Y. Lee, P. Hudek, I. W. Rangelow, G. Stangl, W. Fallmann, *J. Vac. Sci. Technol. B* **1999**, *17*, 3119 – 3121.
[39] K. Arshak, M. Mihov, A. Arshak, D. McDonagh, D. Sutton, *Microelectron. Eng.*, **2004**, *73–74*, 144 – 151.
[40] E. Richter, M. Sebald, L. Chen, G. Schmid, G. Zech, *Semiconductor Fabtech, Issue No. 14*, ICG Publishing, London, **2002**, pp. 137 – 142.
[41] W. H. Brunger, M. Torkler, L. M. Buchmann, *J. Vac. Sci. Technol. B* **1997**, *15*, 2355 – 2357.
[42] S. Hirscher, R. Kaesmaier, W. D. Domke, A. Wolter, H. Loeschner, E. Cekan, C. Horner, M. Zeininger, J. Ochsenhirt, *Microelectron. Eng.* **2001**, *57–58*, 517 – 524.
[43] H. Loeschner, G. Stengl, R. Kaesmaier, A. Wolter, *J. Vac. Sci. Technol. B* **2001**, *19*, 2520 – 2524.
[44] W. H. Brunger, M. Torkler, C. Dzionk, B. D. Terris, L. Folks, D. Weller, H. Rothuizen, P. Vettiger, G. Stangl, W. Fallmann, *Microelectron. Eng.* **2000**, *53*, 605 – 608.
[45] A. Dietzel, R. Berger, H. Grimm, W. H. Brunger, C. Dzionk, F. Letzkus, R. Springer, H. Loeschner, E. Platzgummer, G. Stengl, Z. Z. Bandic, B. D. Terris, *IEEE Trans. Magn.* **2002**, *38*, 1952 – 1954.
[46] A. Dietzel, R. Berger, H. Loeschner, G. Stengl, W. H. Brunger, F. Leizkus, *Adv. Mater.* **2003**, *15*, 1152 – 1155.
[47] W. H. Brunger, C. Dzionk, R. Berger, H. Grimm, A. Dietzel, F. Letzkus, R. Springer, *Microelectron. Eng.* **2002**, *61–62*, 295 – 300.
[48] A. Spiegel, W. H. Brunger, C. Dzionk, P. Schmuki, *J. Vac. Sci. Technol. B* **2002**, *20*, 2713 – 2716.
[49] T. Shibata, K. Suguro, K. Sugihara, T. Nishihashi, J. Fujiyama, Y. Sakurada, *IEEE Trans. Semicond. Manuf.* **2002**, *15*, 183 – 188.
[50] W. He, D. B. Poker, K. E. Gonsalves, N. Batina, *Microelectron. Eng.* **2002**, *65*, 153 – 161.
[51] H. Ryssel, I. Ruge, *Ion Implantation*, Wiley, New York, **1986**.

Received: February 12, 2005
Published online on April 11, 2005

